Nuclear matrix elements for the $0\nu\beta\beta(0^+ \to 2^+)$ decay of ^{76}Ge within the two-nucleon mechanism

Dong-Liang Fang [1,2] and Amand Faessler[3]

[1]*Institute of Modern Physics, Chinese Academy of Science, Lanzhou 730000, China*
[2]*School of Nuclear Science and Technology, University of Chinese Academy of Sciences, Beijing 100049, China*
[3]*Institute for Theoretical Physics, Tübingen University, Tübingen D-72076, Germany*

In this paper, we present the first beyond closure calculation for the neutrinoless double-β decay of ^{76}Ge to the first 2^+ states of ^{76}Se within the two nucleon mechanism. The isospin symmetry restored quasiparticle random-phase approximation method with the charge-dependent-Bonn realistic force is adopted for the nuclear structure calculations. We analyze the structure of the nuclear matrix elements and estimate the uncertainties from our nuclear many-body calculations. We find g_{pp} plays an important role for the calculations, and if quenching is included, suppression for the transition matrix element M_λ is found. Our results for the transition matrix elements are about one order of magnitude larger than previous projected Hartree-Fock-Bogolyubov results with the closure approximation.

I. INTRODUCTION

In the standard model, the nuclear weak decay is interpreted as the low-energy effective theory of the weak interaction. This decay is mediated by the left-handed (L) gauge boson $W^\pm$. The mass of $W^\pm$ are acquired through the spontaneous symmetry breaking by the so-called Higgs mechanism. However, the Yukawa coupling of Higgs particle to neutrinos is absent in the standard model due to the absence of the right-handed (R) neutrinos. The discovery of neutrino masses from oscillation experiments then asks for new physics beyond the standard model. As an extension to standard model, the L-R symmetric model [1–3] introduces the right-handed $SU(2)_R$ gauge symmetry and a heavy right-handed gauge boson from symmetry breaking with extra Higgs bosons at a higher-energy scale beyond electroweak scale. In such a theory, the introduction of lepton number violating neutrino Majorana mass terms together with normal Dirac mass terms gives naturally the tiny neutrino mass through the so-called seesaw mechanism [4]. Such extensions to the standard model could also affect the rare nuclear process called neutrinoless double-β decay ($0\nu\beta\beta$). The participation of right-handed weak gauge bosons will also induce the emission of right-handed leptons. The simultaneous presence of weak currents with both chirality will introduce a momentum term into the neutrino propagator. These terms are not suppressed, such as the mass terms due to the smallness of neutrino mass. The right-handed weak currents will contribute to the decay to the ground states with extra terms and change the electron spectra [5]. Nevertheless, these terms are suppressed by the new physics parameters as well as the electron wave functions for p partial waves. Therefore, they are hindered in normal $0\nu\beta\beta$ decay compared to the neutrino mass mechanisms. On the other hand, the decay to the 2^+ states are dominated by the helicity changing mechanisms ($V + A$

terms, see Ref. [6]). In this sense, the branching ratio of neutrinoless double-β decay to the 2^+ state (hereafter $0\nu\beta\beta(2^+)$, the spin parity of the final states of the decay are included inside the parentheses) could help to reveal the underlying mechanisms of this very rare decay. Nevertheless, experimentally such a process is extremely difficult to observe due to the large $2\nu\beta\beta(0^+)$ background around the position of the $0\nu\beta\beta(2^+)$ Q value. Despite the difficulties, the observation of $0\nu\beta\beta(2^+)$ together with that for the decay to the ground states will determine the underlying mechanisms of the neutrinoless double-β decay and pave our way to new physics beyond the standard model. For example, the observation of $0\nu\beta\beta(2^+)$ could possibly rule out a category of mechanisms where no right-handed gauge bosons or fermions are present.

There are numerous publications dedicated to the nuclear many-body calculations for neutrinoless double-β decay with various approaches, e.g., the shell-model calculations [7,8], the quasiparticle random-phase approximation (QRPA) calculations [9,10], the IBM calculations [11], and the nuclear mean-field calculations [12], especially the recently developed *ab initio* methods [13]. However, all these works focus on $0\nu\beta\beta(0^+)$, and there are not too many theoretical investigations available for the nuclear matrix elements (NMEs) of $0\nu\beta\beta(2^+)$ in the literature. An earlier calculation [14] with the projected Hartree-Fock-Bogolyubov method (PHFB) suggests, that the NMEs for this decay mode are much smaller than for the decay to the ground states. The QRPA method is widely used in double-β decay calculations [10,15,16]. And it can be adopted to describe the vibrational 2^+ states. Therefore, there are attempts to use the QRPA to calculate $\beta\beta$ decays to the first 2^+ state [17–21]. And most of them focus on the $2\nu\beta\beta$ case. There are also calculations with other many-body methods [22,23]. In this paper, we go step forward by carrying out the QRPA calculations for $0\nu\beta\beta(2^+)$

for ^{76}Ge. Taking advantage of the QRPA method, we take into account the contributions from all the intermediate states. Also we can include the isoscalar particle-particle residual interaction which is missing in PHFB calculations. At this first attempt, we do not include too many examples. We focus on one nucleus, ^{76}Ge which is also the candidate treated in Ref. [14]. It has been shown in Ref. [14], that besides the nucleon mechanism, the N* could also play an important role, we will not discuss this in the current paper. Also, as in Ref. [7], the induced weak current will further reduce the NME, this will be neglected in this paper as well as the heavily suppressed neutrino mass mechanism for $0\nu\beta\beta(2^+)$ through nuclear recoil [24].

The current article is arranged as follows: First we give the general formalism of our many-body calculations, and then we show the results and discuss possible uncertainties, and finally we present the conclusions and outlook.

II. FORMALISMS

The half-lives of $0\nu\beta\beta(2^+)$ can be expressed in a simple form, whereas we consider only the light neutrino [6,14],

$$\tau^{-1} = F_1(\langle\lambda\rangle M_\lambda - \langle\eta\rangle M_\eta)^2 + F_2(\langle\eta\rangle M'_\eta)^2. \quad (1)$$

Here $F_{1(2)}$ are the phase-space factors expressed in Refs. [6,14]. $\langle\lambda\rangle$ and $\langle\eta\rangle$ are the new physics parameters which are model dependent. In the L-R symmetric model [2] [such as $\mathrm{SU(2)_L SU(2)_R U(1)_{B-L}}$], we have [6]

$$\langle\lambda\rangle = \lambda \sum_j U_{ej}V_{ej}, \qquad \langle\eta\rangle = \eta \sum_j U_{ej}V_{ej}. \quad (2)$$

Here U_{ej} and V_{ej} are matrix elements for the generalized Pontecorvo-Maki-Nakagawa-Sakata matrix [25]. $\lambda \approx (M_{W\mathrm{L}}/M_{W\mathrm{R}})^2$ are the square of the ratio of the masses between the mass eigenvalues of the light and heavy gauge bosons, $\eta \approx \tan\xi$ is the mixing angle between the left-handed gauge boson and the heavy gauge boson mass eigenstate.

M_λ, M_η, and M'_η are the NMEs which are combinations of different components [6],

$$M_\lambda = \sum_{i=1}^5 C_{\lambda i}M_i, \quad M_\eta = \sum_{i=1}^5 C_{\eta i}M_i, \quad M'_\eta = \sum_{i=6}^7 C'_{\eta i}M_i. \quad (3)$$

The different coefficients C_{Ii} are given in Table I of Ref. [14].

The general form of above NMEs can be expressed within the QRPA framework as

$$M_I = \sum_{J^\pi m_i m_f} \sum_{J' \mathcal{J} \mathcal{J}'} \begin{Bmatrix} j_\mathrm{p} & j_\mathrm{p'} & \mathcal{J} \\ j_\mathrm{n} & j_\mathrm{n'} & \mathcal{J}' \\ J & J' & 2 \end{Bmatrix} \langle j_\mathrm{p}j_\mathrm{p'}\mathcal{J}\|O_I\|j_\mathrm{n}j_\mathrm{n'}\mathcal{J}'\rangle$$

$$\times \frac{(-1)^{J'+J}}{\sqrt{2J'+1}} \langle \widetilde{2_{1f}^+\|[c_\mathrm{p}^\dagger \tilde{c}_\mathrm{n}]_{J'}}\|J^\pi m_f\rangle \langle J^\pi m_f\|J^\pi m_i\rangle$$

$$\times \langle J^\pi m_i\|[c_\mathrm{p}^\dagger \tilde{c}_\mathrm{n}]_J\|0_i^+\rangle. \quad (4)$$

A general derivation of the expressions for above single-particle matrix elements $\langle j_\mathrm{p}j_\mathrm{p'}\mathcal{J}\|lO_I\|j_\mathrm{n}j_\mathrm{n'}\mathcal{J}'\rangle$ are given

in the Appendix. For the related operators, we have the form [14]

$$O_1 = \sigma_1\sigma_2[\hat{r} \otimes \hat{r}]^{(2)}h(r), \quad (5)$$

$$O_2 = [\sigma_1 \otimes \sigma_2]^{(2)}h(r), \quad (6)$$

$$O_3 = ([\sigma_1 \otimes \sigma_2]^{(2)} \otimes [\hat{r} \otimes \hat{r}]^{(2)})^{(2)}h(r), \quad (7)$$

$$O_4 = [\hat{r} \otimes \hat{r}]^{(2)}h(r), \quad (8)$$

$$O_5 = \{(\sigma_1 + \sigma_2) \otimes [\hat{r} \otimes \hat{r}]^{(2)}\}^{(2)}h(r). \quad (9)$$

And,

$$O_6 = \{(\sigma_1 - \sigma_2) \otimes [\hat{r} \otimes \hat{r}_+]^{(1)}\}^{(2)}\frac{r_+}{r}h(r), \quad (10)$$

$$O_7 = \{(\sigma_1 - \sigma_2) \otimes [\hat{r} \otimes \hat{r}_+]^{(2)}\}^{(2)}\frac{r_+}{r}h(r). \quad (11)$$

Here r is the relative distance between the two decaying nucleons $\vec{r} = \vec{r}_1 - \vec{r}_2$ and $\vec{r}_+ = \vec{r}_1 + \vec{r}_2$ is defined in Ref. [14].

Here, $M_1 - M_3$ are the space-space components of the current-current interaction, whereas M_4 is the time-time components, and $M_5 - M_7$ are the time-space components. These time-space components of the NMEs appear only in the L-R symmetric case and are missing in the neutrino mass mechanisms. In all these NMEs, we find a similarity between M_2 and $M_{\mathrm{GT}}^{0\nu}$ for $0\nu\beta\beta(0^+)$ as well as M_3 and $M_T^{0\nu}$. The Gamow-Teller (GT) operator σ or the tensor operator $[\sigma \otimes \hat{r}]^2$ replace the scalar products in $0\nu\beta\beta(0^+)$. We also find an analog similarity between M_4 and $M_F^{0\nu}$, where $\hat{r}$'s come from the p-wave electron and the momentum term form a tensor product instead of a scalar product in $0\nu\beta\beta(0^+)$.

The neutrino potential differs from that of the mass mechanism due to the momentum terms in the neutrino propagator [5],

$$h(r) = \frac{2R}{\pi}r\int \frac{F(q^2)j_1(qr)q^2dq}{q + E_N}. \quad (12)$$

By deriving this, we assume that the two electrons share the decay energy, therefore, $E_N = E_m + M_m - (M_i + M_f)/2$, and E_m is the excitation energy of the mth excited states of the intermediate nucleus. The nuclear radius $R = 1.2A^{1/3}$ (fm) introduced here makes the final NME dimensionless. For the form factor $F(q^2)$ we use a dipole form with the parameters as in Ref. [9].

Usually, an extra radial function $f(r)$ should be multiplied to the above expression to take into consideration the strong repulsive nature of nucleon-nucleon interaction at short range. This is usually called the short-range correlation (src) function, and in our calculation we choose the charge-dependent (CD)-Bonn or Argonne src extracted from the corresponding nuclear force with the form given in Ref. [26].

For the reduced one-body density for transitions from intermediate states to final 2^+, the expression is complicated [27]

$$\frac{\langle 2_f^+ \| [\tilde{c}_p^\dagger c_n]_{J'} \| J^\pi m \rangle}{\sqrt{2J'+1}} = \sqrt{5(2J+1)} \left[\sum_{p' \leqslant p} \frac{(-1)^{j_{p'}+j_n}}{\sqrt{1+\delta_{p'p}}} \begin{Bmatrix} 2 & j_{p'} & j_p \\ j_n & J' & J \end{Bmatrix} \left(u_p u_n \mathcal{X}_{p'p}^{2_f^+} X_{p'n}^{J^\pi m} - v_p v_n \mathcal{Y}_{p'p}^{2_f^+} Y_{p'n}^{J^\pi m} \right) \right.$$

$$+ \sum_{p' \geqslant p} \frac{(-1)^{j_p+j_n}}{\sqrt{1+\delta_{pp'}}} \begin{Bmatrix} 2 & j_{p'} & j_p \\ j_n & 1 & 1 \end{Bmatrix} \left(u_p u_n \mathcal{X}_{pp'}^{2_f^+} X_{p'n}^{m} - v_p v_n \mathcal{Y}_{pp'}^{2_f^+} Y_{p'n}^{m} \right)$$

$$- \sum_{n' \leqslant n} \frac{(-1)^{j_n+j_p}}{\sqrt{1+\delta_{nn'}}} \begin{Bmatrix} 2 & j_{n'} & j_n \\ j_p & 1 & 1 \end{Bmatrix} \left(v_p v_n \mathcal{X}_{n'n}^{2_f^+} X_{pn'}^{m} - u_p u_n \mathcal{Y}_{n'n}^{2_f^+} Y_{pn'}^{m} \right)$$

$$- \sum_{n' \geqslant n} \frac{(-1)^{j_{n'}+j_p}}{\sqrt{1+\delta_{nn'}}} \begin{Bmatrix} 2 & j_{n'} & j_n \\ j_p & 1 & 1 \end{Bmatrix} \left(v_p v_n \mathcal{X}_{nn'}^{2_f^+} X_{pn'}^{m} - u_p u_n \mathcal{Y}_{nn'}^{2_f^+} Y_{pn'}^{m} \right) \right]. \tag{13}$$

Here X's and Y's are the amplitudes for pn-QRPA (proton-neutron quasiparticle random-phase approximation) describing the intermediate states and $\mathcal{X}$'s and $\mathcal{Y}$'s are the amplitudes for charge-conserving (CC)-QRPA describing the final 2^+ state [27]. And u's and v's are the BCS coefficients.

The reduced one-body density for transitions from the initial states to the intermediate states can be expressed as [9]

$$\frac{\langle J^\pi m_i \| [c_p^\dagger \tilde{c}_n]_J \| 0_i^+ \rangle}{\sqrt{2J+1}} = \sum_{pn} \left(u_p v_n X_{pn}^{J^\pi,m_i} + u_n v_p Y_{pn}^{J^\pi,m_i} \right). \tag{14}$$

We also introduce the overlap between the initial and the final intermediate states with the form [9],

$$\langle J^\pi m_f \| J^\pi m_i \rangle = \sum_{pn} \left(X_{pn}^{J^\pi,m_i} X_{pn}^{J^\pi,m_f} - Y_{pn}^{J^\pi,m_i} Y_{pn}^{J^\pi,m_f} \right)$$

$$\times \left(u_p^i u_p^f + v_p^i v_p^f \right) \left(u_n^i u_n^f + v_n^i v_n^f \right) {}_f \langle \mathrm{BCS} | \mathrm{BCS} \rangle_i. \tag{15}$$

For simplicity, we set ${}_f \langle \mathrm{BCS} | \mathrm{BCS} \rangle_i \approx 1$.

The details of derivations of the BCS coefficients and respective QRPA amplitudes for the current paper are presented in Ref. [27].

III. RESULTS AND DISCUSSION

For our QRPA calculations, the single-particle energies are taken from the solutions of Schrödinger equations with a Coulomb corrected Woods-Saxon potential. For the single-particle wave functions, we use the harmonic-oscillator wave functions. For the pairing part, we use the realistic CD-Bonn force derived from the Brückner G matrix. This is also used for the pn-QRPA and CC-QRPA residual interactions. A fine-tuning of the interactions is needed to reproduce the experimental values. For the pairing part, we fit the two parameters g_{pair}^p and g_{pair}^n to reproduce the odd-even mass staggering. For pn-QRPA, we multiply the G matrix by overall renormalization factors g_{ph} and g_{pp}'s for particle-hole and particle-particle parts, respectively. We set $g_{\mathrm{ph}} = 1$. And for g_{pp}, we fit the isoscalar channel ($g_{\mathrm{pp}}^{T=0}$) and isovector channel ($g_{\mathrm{pp}}^{T=1}$) separately. $g_{\mathrm{pp}}^{T=0}$ is fixed by reproducing the experimental $2\nu\beta\beta$ and $g_{\mathrm{pp}}^{T=1}$ are fixed to put to zero the $2\nu\beta\beta$

Fermi matrix elements due to isospin symmetry restoration [28]. For more details, one can refer to the our previous work [27]. For a baseline calculation, we consider the CD-Bonn src and the bare axial vector coupling constant $g_{A0} = 1.27$. And we use the model space with $N_{\max} = 6$ which consists of 28 single-particle levels for both neutrons and protons.

In Table I, we present the NMEs for each operator. As a comparison, we also present the results from PHFB calculations. The current results (the baseline results) differ from the PHFB results by factors from five to more than one order of magnitude case by case. The largest deviation we see in M_7 for the M'_η part. We obtain M_7 much larger than M_6 in magnitude. Our results have also different phases for these two NMEs, this then combined with the C'_η coefficients leads to the enhancement instead of the reductions of M'_η. Therefore, our M'_η is much larger than a previous PHFB calculation. Although PHFB gets an approximate cancellation between M_6 and M_7, which leads to an negligible M'_η.

For the $M_{\lambda(\eta)}$ part, we find the NMEs have basically similar phases as the PHFB results except for M_2. On the other hand, our results are about one order of magnitude larger, although the relative ratios among different NMEs ($M_1 - M_5$) are similar. Of these NMEs, M_1 is the largest. The second largest is M_2, and third is M_4. M_3 and M_5 are relatively small and, hence, less important. For M_λ, if we multiply the NMEs with the corresponding C_λ's, we find that M_1 and M_2 contributes coherently, they are then canceled by M_4, whereas the remaining two NMEs contributes less than 10%. For M_η, all these three NMEs give additive contributions, this makes M_η about three times larger than M_λ. This is the reason why M_η is larger than M_λ as also observed in Ref. [14]. However, in their calculation, the strong cancellation gives a negligible M_λ, the ratio of M_η to M_λ is about 30. In short, in their calculation, only M_η is important whereas M_λ and M'_η can be neglected due to the cancellations between different parts of the NME. We get quite different results, and M'_η is the most important contribution with a value about three times larger than M_η. This will affect the constraints on new physics models and needs further investigation.

As we show above, no obvious suppression of $0\nu\beta\beta(2^+)$ NMEs as claimed by Ref. [14] is found from

TABLE I. The NME values for $0\nu\beta\beta(2+)$. Here the baseline calculation is explained in the text. And various approximations and parameters will be discussed in the text.

	M_1	M_2	M_3	M_4	M_5	M_λ	M_η	M_6	M_7	M'_η
PHFB [14]	0.151	0.027	−0.002	−0.049	−0.004	0.002	0.061	0.074	0.042	0.001
Baseline	0.705	−0.253	−0.046	−0.153	−0.048	0.150	0.469	0.527	−1.270	1.519
$N_{\max} = 5$	0.629	−0.208	−0.014	−0.124	−0.069	0.151	0.438	0.661	−1.369	1.688
$N_{\max} = 7$	0.640	−0.256	−0.048	−0.145	−0.063	0.121	0.439	0.643	−1.251	1.564
Without src	0.701	−0.234	−0.049	−0.154	−0.051	0.128	0.451	0.485	−1.182	1.410
Argonne src	0.705	−0.250	−0.046	−0.153	−0.048	0.149	0.467	0.519	−1.261	1.505
Leading order	0.749	−0.347	−0.051	−0.154	−0.041	0.228	0.540	0.823	−1.756	2.152
Without $F(q^2)$	0.695	−0.241	−0.047	−0.154	−0.050	0.136	0.457	0.529	−1.272	1.521
Closure energy	0.696	−0.267	−0.043	−0.144	−0.041	0.177	0.472	0.522	−1.247	1.493
$g_{\mathrm{pp}}^{T=0} = 0$	0.611	−0.169	−0.054	−0.161	−0.065	0.029	0.376	0.540	−1.240	1.496
$g_{\mathrm{pp}}^{T=1} = 0$	0.795	−0.246	−0.034	−0.156	−0.034	0.206	0.516	0.501	−1.437	1.665
$g_A = 0.75$	0.695	−0.241	−0.047	−0.154	−0.050	0.008	0.317	0.529	−1.272	1.249

current calculations compared to $0\nu\beta\beta(0^+)$, this also agrees with the q terms in $0\nu\beta\beta(0^+)$ calculations [29]. This is the major difference of the current paper and Ref. [14]. This is also different from $2\nu\beta\beta(2^+)$ where the NME is suppressed by the cubic dependence of the energy denominator [6]. In this sense, suppression of $0\nu\beta\beta(2^+)$, if it exists, must be related to other issues. This may come from the uncertainties of the many-body approaches, such as the size of the model space or other structure ingredients for the 2^+ states which may lead to different transition rates from the intermediate states for various transitions. A more thorough comparative study could give us more detailed hints.

Compared to previous calculations with PHFB [14], the QRPA calculation goes beyond the closure approximation (see Ref. [30]). We calculate explicitly the contribution from each intermediate state. In Figs. 1–4, we present the individual contributions from different multipoles of the intermediate states, and we will also show how the different approximations may affect these results. In each graph, the results are compared with our present baseline calculations with standard conditions described above.

For details of the structure of the nuclear MMEs, we start with our baseline calculation (e.g., orange bars in Fig. 1). For M_1, the multipoles give positive contributions with several exceptions. Unlike $0\nu\beta\beta(0^+)$ ($M_{\mathrm{GT}}^{0\nu}$) where the largest contributions come from low-spin intermediate states and the NME values decrease as spins increase, M_1 has its largest contribution from 4^-. We find a rough trend that the NMEs first increase and then decrease as spin increases. And as one would expect, the NMEs from states with very high spin can be safely neglected. M_2 has basically the same characters as M_1 except the much smaller magnitude. A large contribution from 1^- is observed for M_2 but not for M_1. For most multipoles, M_2 has different signs as M_1, this contradicts conclusions in Ref. [14]. Not all multipoles contribute equally with similar spins, we find that the states with negative parity generally contribute more. In some sense, these two NMEs behave like $M_{\mathrm{GT}}^{0\nu}$ for $0\nu\beta\beta(0^+)$ as we mentioned above. The smallness of final M_3 comes partially from its magnitude and partially from the cancellations between low-spin and

high-spin multipoles. This is in analog with $M_T^{0\nu}$, although these two NMEs depend differently on $\hat{r}$. M_4, the time-time component of the NME is, on the other hand, very close to $M_F^{0\nu}$. These two NMEs have one thing in common: Only intermediate states with natural parity $[\pi = (-1)^J]$ have nonzero contributions. In the current calculation, all multipoles contribute negatively except 1^-.

For the space-time components, $M_5 - M_7$, we find a quite different behavior. The values of M_5 from each multipole is about one order of magnitude smaller than M_6 and M_7. Due to the strong cancellations among different multipoles, M_5 is one of the smallest of all the NMEs. For M_6, almost all multipoles contribute positively except a strong cancellation from 3^-. For M_7, the important contributions comes from three multipoles (3^-, 5^-, and 7^-), all the other multipoles contribute much less. The lack of cancellations from other multipoles thus makes M_7 the largest from all the NMEs.

A possible cause of the smallness of NMEs in Ref. [14] may come from the small model space with only two major shells. To test this, we plot in Fig. 1 the results with $N_{\max} = 5$ (blue bars) and $N_{\max} = 7$ (green bars). The sensitivity of the NME to different model spaces is different. Also the sensitivity of the individual multipoles for each NME is different. For M_1, the influence from model space is generally small, there is no unique trend for different multipoles under the change in the model space. For some multipoles, the NME decreases with enlarged model space, but most cases we find that the addition of extra orbitals will first enhance but then reduce the NME. The orbitals of different parities contribute to the NME differently. The addition of $N = 6$ shell brings in the positive-parity orbitals which enhance the NMEs for multipoles, such as 3^- or 5^+, whereas the negative-parity orbitals from $N = 7$ shells reduce the NMEs. Unlike the case of M_1, the increase in the model space enlarge M_2, especially for 1^+, 2^-, etc. For 1^+, a strong suppression is observed when the $N = 6$ shell is added. But such addition gives strong enhancement to 2^- or 3^+. The addition of the $N = 7$ shell to the model space causes milder changes. We see enhancement from 1^- and 2^- but reductions from 3^- and 4^- intermediate states. A similar behavior works for the M_3 where we find a strong
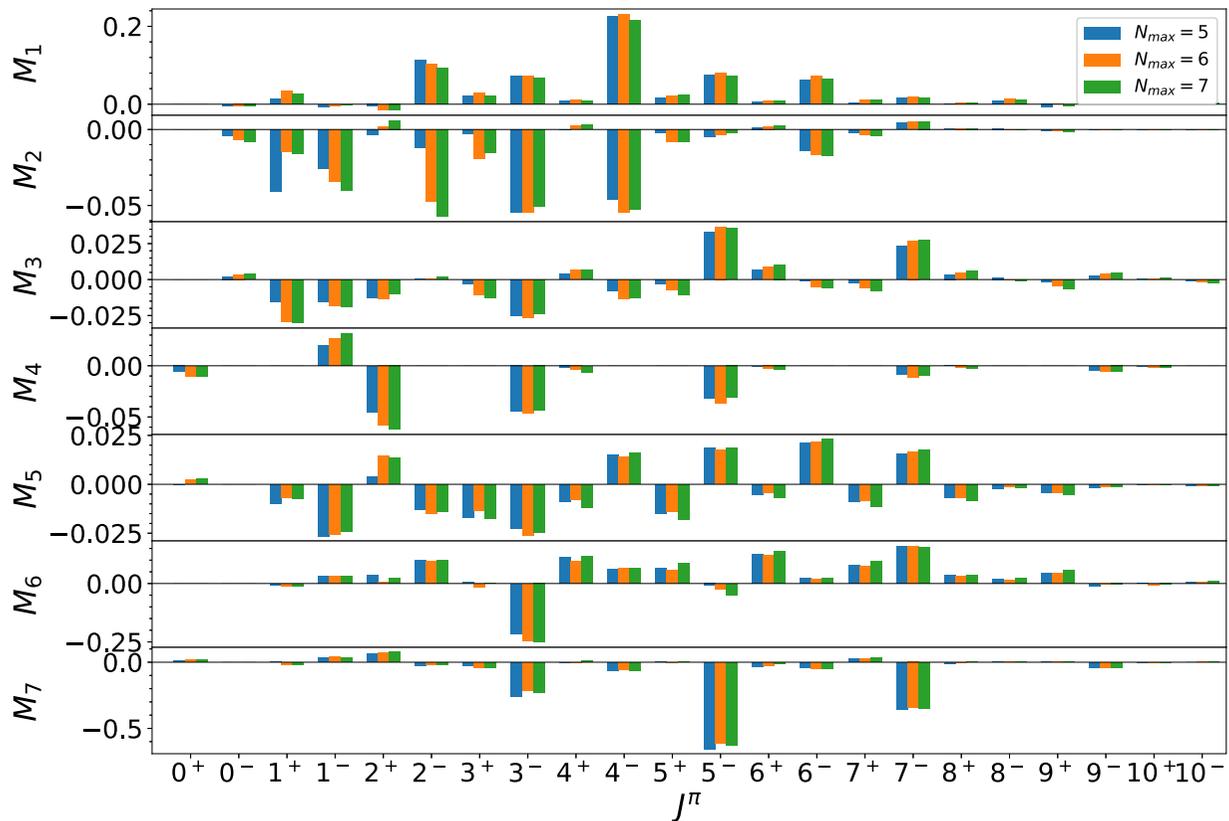
FIG. 1. The dependence of the NMEs on the model space for different multipoles. Here $N_{\max}$ refers to the largest principal quantum number for the outermost shell.

enhancement from 1^+ too. For all other multipoles, the change due to model space enlargement is relatively small. For M_4, low-spin multipoles are much more sensitive to the model space changes, and different multipoles behave differently, although we cannot find any specific patterns. This is also true for the space-time components of the NME. In general, they are less affected by the change in model space in our calculations.

If we look at the total changes in each NME from $N_{\max} = 5$ to $N_{\max} = 6$, M_1 increases about 10%. This is the smallest change among all the NMEs. Meanwhile, all the other NMEs change about 20% or more. By percentage M_3 changes by more than 200%. By the absolute values of NMEs, $M_1 - M_4$ get enhanced whereas the rest get reduced. When the $N = 7$ shell is added, the change is relatively milder, especially for $M_2 - M_4$, this implies a general trend of convergence of the results with a larger model space. But for M_1, $M_5 - M_7$, we find a slower trend of convergence than for the above NMEs. In either cases, the changes from adding the $N = 7$ shell is smaller than adding the $N = 6$ shell. Current results suggest that the errors of adopting the current model space are generally smaller than 20%. Also, these results suggest that the deviation of our calculations and those in Ref. [14] is probably not caused by the small model space, which they adopted. It is most probable that the smallness of their results are caused by different structures from the calculations. Additional work is needed to clarify this.

The form factor with a dipole form is widely used in $0\nu\beta\beta(0^+)$ calculations [9]. In our calculations, we use the same form for $g_V(q^2)$ and $g_A(q^2)$. We find that the form factors are not very important except for the 1^+ states of M_2. This may suggest that with the actual neutrino potential, the low-momentum parts where the q^2 satisfies $g_A(q^2) \approx g_A(0)$ dominate, and the high-momentum parts are either small or cancel each other. A careful check suggests the latter should apply in QRPA calculations. These behaviors also help to explain the large reduction for some NMEs when the realistic neutrino potential is considered. With low momenta, the intermediate energies may become important. In this sense, the choice of the intermediate energies becomes important. For calculations with closure approximation, a closure energy is needed. So we also check how the usage of closure energy would affect the NMEs. This is illustrated with the red bars in Fig. 2 where a closure energy of 7 MeV is used. We find for most multipoles of most NMEs, the proper choice of closure energy brings small errors to the calculation, and we can draw the conclusion, that using the closure energy in $0\nu\beta\beta(2^+)$ barely changes the final results, the errors are within several percentages, and this agrees with $0\nu\beta\beta(0^+)$ QRPA calculations. Another important correction comes from the induced weak current [9], it is not included in the current calculations and will be implemented in our future study. If that is included, the NME will most probably be further reduced, and new potentials also need to be introduced [5].
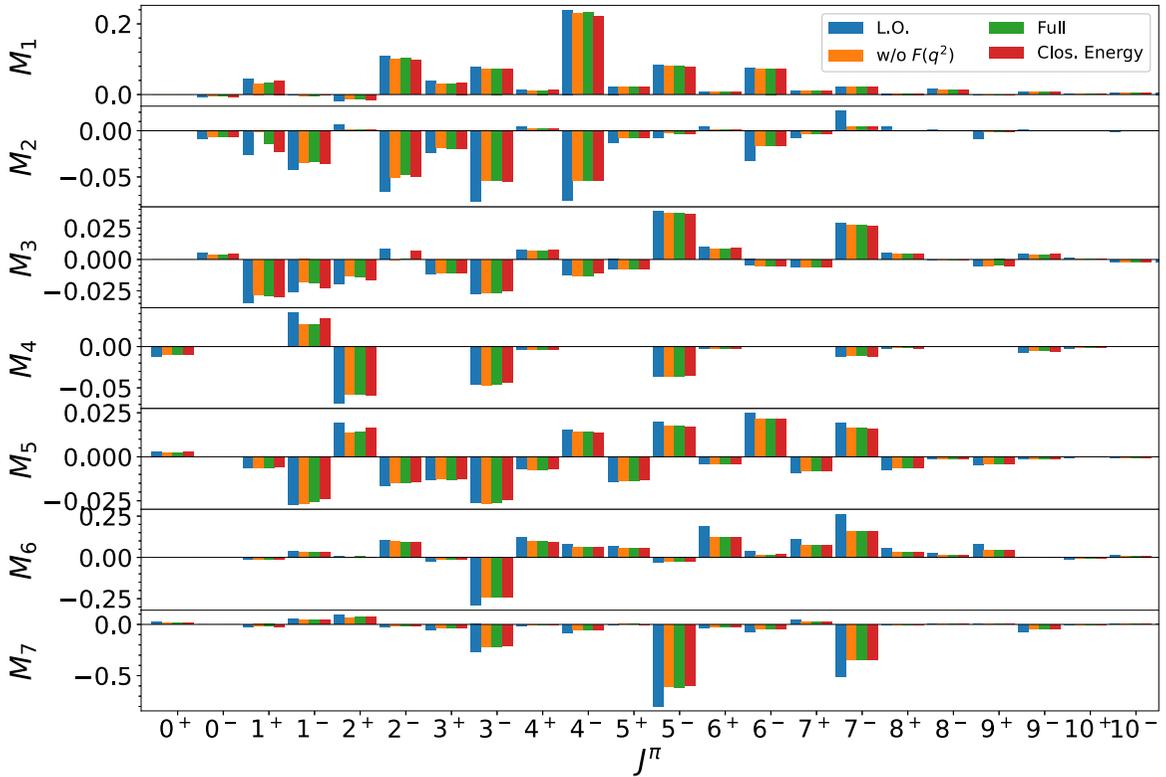
FIG. 2. The NMEs for a Coulomb-type neutrino potential (blue bars). The orange bars are NMEs without form factors and the red bars are with excitation energies replaced by a closure energy. The green bars are our baseline calculations explained in the text.

In $0\nu\beta\beta(0^+)$, src plays an important role for the heavy neutrino mass mechanism [12,31], whereas for the light neutrino mass mechanism, the correction is relatively small, up to only several percentages [12,31]. In current calculations, we adopt two srcs [26]: The CD-Bonn type and Argonne type, they are obtained by fitting the respective nuclear potentials. From Fig. 3, we find similar trends as $0\nu\beta\beta(0^+)$, the general correction from the src is about several percentages, and for most cases, the two srcs give similar amounts of corrections. For almost all multipoles, we find that the src enhances the NMEs more or less. However, the net effects to the NMEs are slight reductions for M_3 and M_5 due to cancellations among different multipoles. And enhancements of NME values for other operators are observed. The largest correction comes from M_6, then M_7 and M_2. For M_6 we can also find a slight difference between the two srcs.

The most important parameters in QRPA calculations are the particle-particle interaction strength $g_{\rm pp}$'s. For $0\nu\beta\beta(0^+)$, one finds that $M_{\rm GT}$ for both $2\nu\beta\beta$ and $0\nu\beta\beta$ depends sensitively on the isoscalar strength $g_{\rm pp}^{T=0}$ whereas $M_F^{0\nu}$'s are sensitive to the isovector strength $g_{\rm pp}^{T=1}$. So we also test such dependence in current calculations. As we have shown in Ref. [27] for the case of $2\nu\beta\beta$ to 2^+ states, the GT-type decays are also sensitive to $g_{\rm pp}^{T=1}$ since the isovector particle-particle residue force affects the structure of 2^+ states in QRPA calculations. In Fig. 4, we first switch off the isoscalar interaction (the blue bar). Then the effects of this interaction to NMEs can be estimated by comparing the blue and green

bars. The results suggest that, whereas M_6 and M_7 are not closely related to $g_{\rm pp}^{T=0}$, M_2 comes out to be the most sensitive one like its $0\nu\beta\beta(0^+)$ counterpart $M_{\rm GT}^{0\nu}$. Similar as $M_{\rm GT}^{0\nu}$, 1^+ comes out to be the most sensitive multipole, the increase in the $g_{\rm pp}^{T=0}$ drastically changes the NME most probably due to the SU(4) symmetry restoration [28]. And the effects of isoscalar residue interactions to the specific multipoles of specific NMEs are quite different, some NMEs are enhanced, and some are reduced. In total, the introduction of isoscalar interactions enhances M_1, M_2, and M_7 but reduces other NMEs. And the magnitudes of these enhancements and reductions are really case dependent. The similar thing happens to isovector interactions (this interaction has been switched off for the red bars in Fig. 4) for some cases they are more important than the isoscalar interactions. In general, the particle-particle interaction is one of the most important source of the errors for QRPA calculations. M_4 is, at least, sensitive to $g_{\rm pp}$'s whereas M_2 and M_7 are really sensitive to $g_{\rm pp}^{T=0}$ and $g_{\rm pp}^{T=1}$ respectively. Especially M_2, the absence of isoscalar interactions will reduce the NME by more than 30%.

The special attention should be paid to the case of the quenched g_A. In all our above analyses, we assume that g_A is not quenched, however, in nuclear medium quenching of g_A is observed. In current calculations, we use the simplest treatment for quenching, that is simply change the value of g_A, whereas there exists more fundamental approaches for the quenching of g_A using the chiral two-body currents [32]. In our case, the difference between quenched g_A calculations
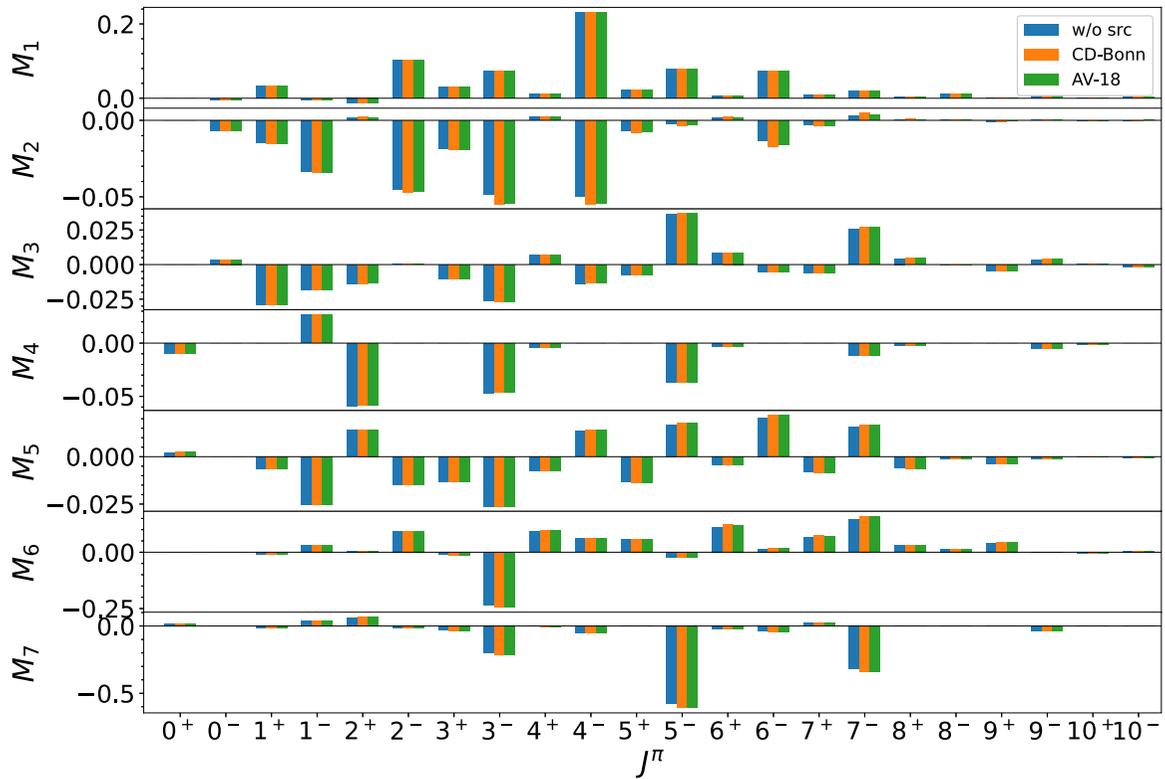
FIG. 3. The NME dependence on the short-range correlations.
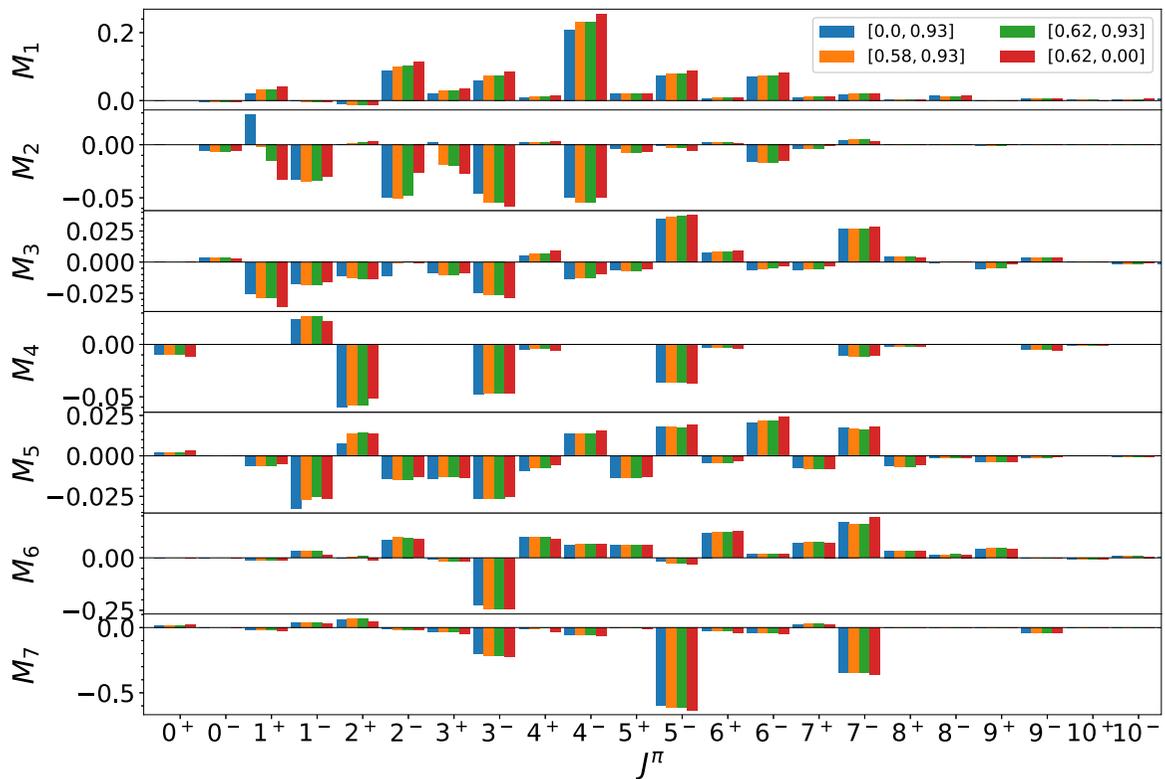
FIG. 4. The NME dependence on g_{pp}'s. The values in the bracket are $g_{pp}^{T=0}$ and $g_{pp}^{T=1}$, respectively. The blue bars are results with $g_{pp}^{T=0} = 0$, and the orange bars are $g_{pp}^{T=0}$ values which reproduce the $2\nu\beta\beta$ NME with $g_A = 0.75g_{A0}$. The red bars are results with $g_{pp}^{T=1} = 0$. And the green bars here again are the baseline calculations.

and our baseline calculations are the different fits of $g_{\mathrm{pp}}^{T=0}$. Therefore, the difference for the individual NMEs are small as in Fig. 4. But the quenched g_A will also change the coefficient C's. As a result, the NMEs M_λ, M_η, and M'_η have been changed too. In general, these NMEs are reduced due to the convention used in Ref. [14]. For M'_η, a reduction of a rough factor of g_A/g_{A0} is expected since the two components M_6 and M_7 have the same dependence on g_A. For M_λ and M_η, different components have a different g_A dependence. And if we take $g_A = 0.75g_{A0}$ we find a rough cancellation for M_λ as also predicted in Ref. [14], this comes from the interplay among different components. Meanwhile the reduction for M_η is basically 25%. The severe reductions of M_λ emphasize the importance of where the quenching of g_A originates and how to treat it properly.

IV. CONCLUSION AND OUTLOOK

In this paper, we calculate the NME of $0\nu\beta\beta$ to 2_1^+ for ^{76}Ge. We got quite large results compared to previous calculations. We estimate the errors of current calculation by changing several parameters we use. We find that g_A may be a very important issue for the final NMEs. Further investigations, such as the role of the induced weak current, the anharmonicity beyond QRPA, and the decay mechanism mediated by N*, are needed for much more detailed conclusions.

ACKNOWLEDGMENTS

APPENDIX: DERIVATION OF SINGLE-PARTICLE MATRIX ELEMENTS IN THE PARTICLE-PARTICLE CHANNEL

The seven $0\nu\beta\beta(2^+)$ decay operators are taken from Ref. [14] and presented above. They can be written in the forms of combination of three parts: the relative coordinate $[O^r(\vec{r}) \equiv O_J(\hat{r})h(r)]$, the center-of-mass coordinate $[O^{r_+}(\vec{r}_+) \equiv O_J(\hat{r}_+)f(r_+)]$ and the spin part $[O^S(\vec{\sigma}_1, \vec{\sigma}_2)]$. These operators can then be expressed in a general form $O_I^{(2)} = \{[O_{J_1}(\hat{r}) \otimes O_{J_2}(\hat{r}_+)]^{(J')} \otimes O_{J_3}(\vec{\sigma}_1, \vec{\sigma}_2)\}^{(2)}h(r)f(r_+)$.

We assume the quantum numbers for the single orbital are (n_1, l_1, j_1) and (n_2, l_2, j_2) for protons and $(\mathrm{n}'_1, l'_1, j'_1)$ and $(\mathrm{n}'_2, l'_2, j'_2)$ for neutrons. The single matrix elements of these operators under the harmonic-oscillator basis can be expressed as

$$\langle \mathrm{pp}'\mathcal{J} \| \{[O_{J_1}(\hat{r}) \otimes O_{J_2}(\hat{r}_+)]^{(J')} \otimes O_{J_3}(\vec{\sigma}_1, \vec{\sigma}_2)\}^{(2)} \| \mathrm{nn}'\mathcal{J}' \rangle$$
$$= \sum_{nl\mathcal{NLLS}} A_{\mathrm{pp}'\mathcal{J},\mathrm{LS}} \langle \mathrm{n}_1l_1, \mathrm{n}_2l_2, L | nl\mathcal{NL}, L\rangle$$
$$\times \sum_{n'l'\mathcal{N'L'L'S'}} A_{\mathrm{nn}'\mathcal{J}',\mathrm{L'S'}} \langle \mathrm{n}'_1l'_1, \mathrm{n}'_2l'_2, L' | n'l'\mathcal{N'L'}, L'\rangle$$
$$\times \langle nl\mathcal{NLL}; s_1, s_2, S; \mathcal{J} \| O_I^{(2)} n'l'\mathcal{N'L'L'}; s'_1, s'_2, S'; \mathcal{J}'\rangle. \tag{A1}$$

Here $A_{\mathrm{pp}'(\mathrm{nn}')J,\mathrm{LS}}$ is the $9j$ symbol for JJ to LS coupling transformations,

$$A_{\tau\tau'J,\mathrm{LS}} = (2S+1)(2L+1)\sqrt{(2j_\tau+1)(2j_{\tau'}+1)}$$
$$\times \begin{Bmatrix} \frac{1}{2} & l_\tau & j_\tau \\ \frac{1}{2} & l_{\tau'} & j_{\tau'} \\ S & L & J \end{Bmatrix}. \tag{A2}$$

And $\langle \mathrm{n}_1l_1, \mathrm{n}_2l_2, L | nl\mathcal{NL}, L\rangle$ is the Brody-Moshinski transformation coefficients [33].

Using techniques from, e.g., Ref. [34], we could further get the expressions of each operator,

$$\langle nl\mathcal{NLL}; s_1, s_2, S; \mathcal{J} \| O_I^{(2)} \| n'l'\mathcal{N'L'L'}; s'_1, s'_2, S'; \mathcal{J}'\rangle$$
$$= \sqrt{5(2\mathcal{J}+1)(2\mathcal{J}'+1)} \begin{Bmatrix} L & L' & J' \\ S & S' & J_3 \\ \mathcal{J} & \mathcal{J}' & 2 \end{Bmatrix}$$
$$\times \sqrt{(2\mathcal{J}+1)(2\mathcal{J}'+1)(2J'+1)} \begin{Bmatrix} l & l' & J_1 \\ \mathcal{L} & \mathcal{L}' & J_2 \\ L & L' & J' \end{Bmatrix}$$
$$\times \langle nl \| O_{J_1}(\hat{r})f(r) \| n'l'\rangle \langle \mathcal{NL} \| O_{J_2}(\hat{r}_+)f(r_+) \| \mathcal{N'L'}\rangle$$
$$\times \langle s_1, s_2, S \| O_{J_3}(\vec{\sigma}_1, \vec{\sigma}_2) \| s'_1, s'_2, S'\rangle. \tag{A3}$$

All these reduced matrix elements with different $O_{J_1}(\hat{r})$'s, etc., can be calculated analytically in harmonic-oscillator basis, and we omit their derivations in current article, one could refer to references, such as Ref. [34].

[1] J. C. Pati and A. Salam, Phys. Rev. D **10**, 275 (1974).

[2] R. Mohapatra and J. C. Pati, Phys. Rev. D **11**, 2558 (1975).

[3] G. Senjanovic and R. N. Mohapatra, Phys. Rev. D **12**, 1502 (1975); R. N. Mohapatra and G. Senjanovic, Phys. Rev. Lett. **44**, 912 (1980); Phys. Rev. D **23**, 165 (1981).

[4] S. F. King, Rep. Prog. Phys. **67**, 107 (2004).

[5] D. Stefanik, R. Dvornicky, F. Simkovic, and P. Vogel, Phys. Rev. C **92**, 055502 (2015).

[6] M. Doi, T. Kotani, and E. Takasugi, Prog. Theor. Phys. Suppl. **83**, 1 (1985).

[7] E. Caurier, F. Nowacki, A. Poves, and J. Retamosa, Nucl. Phys. A **654**, 973c (1999); J. Menendez, A. Poves, E. Caurier, and F.

Nowacki, *ibid.* **818**, 139 (2009); E. Caurier, F. Nowacki, and A. Poves, Phys. Lett. B **711**, 62 (2012).

[8] J. Menéndez, J. Phys. G: Nucl. Part. Phys. **45**, 014003 (2018).

[9] F. Simkovic, G. Pantis, J. D. Vergados, and A. Faessler, Phys. Rev. C **60**, 055502 (1999).

[10] F. Šimkovic, V. Rodin, A. Faessler, and P. Vogel, Phys. Rev. C **87**, 045501 (2013).

[11] J. Barea, J. Kotila, and F. Iachello, Phys. Rev. C **87**, 014315 (2013); **91**, 034304 (2015).

[12] L. S. Song, J. M. Yao, P. Ring, and J. Meng, Phys. Rev. C **90**, 054309 (2014); J. M. Yao, L. S. Song, K. Hagino, P. Ring, and J. Meng, *ibid.* **91**, 024316 (2015); L. S. Song, J. M. Yao, P. Ring, and J. Meng, *ibid.* **95**, 024305 (2017).

[13] J. M. Yao, B. Bally, J. Engel, R. Wirth, T. R. Rodríguez, and H. Hergert, Phys. Rev. Lett. **124**, 232501 (2020).

[14] T. Tomoda, Nucl. Phys. A **484**, 635 (1988).

[15] M. T. Mustonen and J. Engel, Phys. Rev. C **87**, 064302 (2013).

[16] J. Hyvärinen and J. Suhonen, Phys. Rev. C **91**, 024613 (2015).

[17] J. Suhonen and O. Civitarese, Phys. Lett. B **308**, 212 (1993).

[18] M. Aunola and J. Suhonen, Nucl. Phys. A **602**, 133 (1996).

[19] S. Stoica and I. Mihut, Nucl. Phys. A **602**, 197 (1996).

[20] J. Schwieger, F. Simkovic, A. Faessler, and W. A. Kaminski, J. Phys. G: Nucl. Part. Phys. **23**, 1647 (1997).

[21] J. Schwieger, F. Simkovic, A. Faessler, and W. A. Kaminski, Phys. Rev. C **57**, 1738 (1998).

[22] M. Horoi, S. Stoica, and B. A. Brown, Phys. Rev. C **75**, 034303 (2007).

[23] Y. K. Singh, R. Chandra, P. K. Raina, and P. K. Rath, Eur. Phys. J. A **53**, 244 (2017).

[24] T. Tomoda, Phys. Lett. B **474**, 245 (2000).

[25] Z.-z. Xing, Phys. Rev. D **85**, 013008 (2012).

[26] F. Simkovic, A. Faessler, H. Muther, V. Rodin, and M. Stauf, Phys. Rev. C **79**, 055501 (2009).

[27] D. L. Fang and A. Faessler, Chin. Phys. C **44**, 084104 (2020).

[28] V. Rodin and A. Faessler, Phys. Rev. C **84**, 014322 (2011).

[29] K. Muto, E. Bender, and H. V. Klapdor, Z. Phys. A **334**, 187 (1989).

[30] D. L. Fang, A. Faessler, V. Rodin, and F. Simkovic, Phys. Rev. C **83**, 034320 (2011).

[31] D. L. Fang, A. Faessler, and F. Simkovic, Phys. Rev. C **97**, 045503 (2018).

[32] J. Engel, F. Simkovic, and P. Vogel, Phys. Rev. C **89**, 064308 (2014).

[33] M. Moshinsky, Nucl. Phys. **13**, 104 (1959).

[34] A. R. Edmonds, *Angular Momentum in Quantum Mechanics* (Princeton University Press, Princeton, NJ, 1996).